

High throughput evaluation of perovskite-based anode catalysts for direct methanol fuel cells

Kishori Deshpande^a, Alexander Mukasyan^b, Arvind Varma^{c,*}

^a 66-513, Department of Chemical Engineering, 25 Ames Street, MIT Cambridge, MA 02142, USA

^b Department of Chemical and Biomolecular Engineering, University of Notre Dame, Notre Dame, IN 46556, USA

^c School of Chemical Engineering, Purdue University, West Lafayette, IN 47907-2100, USA

Received 16 June 2005; received in revised form 9 September 2005; accepted 12 September 2005

Available online 9 November 2005

Abstract

Liquid feed direct methanol fuel cells (DMFC) are promising candidates for portable power applications. However, owing to the problems associated with expensive Pt-based catalysts, viz., CO poisoning, a promising approach is to use complex oxides of the type ABO_3 (A = Sr, Ce, La, etc. and B = Co, Fe, Ni, Pt, Ru, etc.).

In the current work, a variety of ABO_3 and A_2BO_4 type non-noble and partially substituted noble metal high surface area compounds were synthesized by an effective and rapid aqueous combustion synthesis (CS). Their catalytic activity was evaluated by using “High Throughput Screening Unit”—NuVant System, which compares up to 25 compositions simultaneously under DMFC conditions. It was found that the Sr-based perovskites showed performance comparable with the standard Pt–Ru catalyst. Further, it was observed that the method of doping $SrRuO_3$ with Pt influenced the activity. Specifically, platinum added during aqueous CS yielded better catalyst than when added externally at the ink preparation stage. Finally, it was also demonstrated that the presence of $SrRuO_3$ significantly enhanced the catalytic properties of Pt, leading to superior performance even at lower noble metal loadings.

© 2005 Elsevier B.V. All rights reserved.

Keywords: Direct methanol fuel cells; Anode catalysts; High throughput testing

1. Introduction

Liquid feed direct methanol fuel cells (DMFC) are promising candidates for portable power applications [1]. The various cell components include porous electrodes, a Nafion electrolyte membrane, and bipolar plates. Catalyst deposited on the porous electrodes helps to convert the fuel into benign by-products, H_2O and CO_2 , along with generation of electricity. Currently, Pt-based catalysts are the only materials that exhibit high rates of methanol oxidation at PEM fuel cell operating temperature ($\sim 80^\circ C$). However, platinum is not only expensive, but is also prone to poisoning due to the formation of intermediate species, such as carbon monoxide, during the process [2].

One promising approach to overcome these problems is to use nanoscale *complex oxides* (e.g. perovskites, cuprates, etc.)

instead of conventional noble metal-based *anode catalysts* in the DMFC [3–6]. Note that this idea may involve both complete and partial Pt/Ru replacement in the catalyst composition. In the latter case, it would also lead to Pt loading reduction, which should be 0.2 mg cm^{-2} or less to meet application needs [7]. For example, high surface area perovskite electrocatalysts with the general composition ABO_3 (A = Sr, Ce, La, etc. and B = Co, Fe, Ni, Pt, Ru, Pd, etc.) are attractive candidates for this application. The characteristic feature of these compounds is that there are numerous possible combinations of A and B cations. Substitutions on one or both sites offer the opportunity to manipulate the defect chemistry of the system. In particular, it is well documented [3] that cation substituents incorporated into the perovskite B-lattice have great influence on the overall electrocatalytic activity towards promoting a specific electrochemical reaction. Thus, for efficient and systematic exploration of chemical space for signs of desired chemical activity, one needs to employ: (a) *efficient method for synthesis* of such nanoscale materials with desired composition and purity; (b) *high throughput screening*

* Corresponding author. Tel.: +1 765 494 4075; fax: +1 765 494 0805.
E-mail address: avarma@ecn.purdue.edu (A. Varma).

technique, which allows testing the materials for catalytic activities under conditions close to those in a fuel cell. This feature assumes importance given the wide variety of compositions that map the chemical space. In this context, note that most catalyst performance data reported in the literature refers to using either cyclic voltammetry (cf. [8–11]) or single fuel cell tests (cf. [12–14]). While the latter use conditions similar to observed working parameters, it is a time-intensive process. Specifically, following this approach, ranking of four catalysts may take up to 6 months using a conventional device [15]. For cyclic voltammetry, the measurements are made using a different electrolyte, typically sulfuric acid, and hence may not necessarily reflect its behavior in a fuel cell.

In the current work, we exploit a novel combinatorial-type approach, which involves *rapid synthesis* of numerous compositions followed by a *high throughput measurement* of their performance in real fuel cell conditions. Specifically, we use aqueous combustion synthesis (CS) for rapid preparation of nanoscale oxides. The details of this method are available elsewhere [16–19]. The catalytic activity of the obtained high surface area complex oxide powders was evaluated by using “High Throughput Screening Unit”—*NuVant System*, which allows simultaneous comparison for 25 different compositions under DMFC conditions [15].

In this work, a variety of catalysts were synthesized and evaluated over a wide range of temperature (60–90 °C) and methanol flow rate (1–15 ml min⁻¹) conditions. A comparison of the results with standard Pt–Ru catalyst revealed that partially substituted Sr-based perovskite exhibited promising performance.

2. Experimental procedure

As noted in Section 1, the catalyst selection approach involved two steps: (a) rapid synthesis of numerous compositions using the aqueous combustion synthesis, and (b) rapid screening of their catalytic activity using the NuVant system. The experimental procedure used for each step is described below separately.

2.1. Catalyst synthesis

Aqueous (solution) combustion synthesis (CS) is an attractive technique for the production of different oxides, including ferrites, perovskites and zirconia (cf. [16–20]). It involves a self-sustained reaction between an oxidizer (e.g. metal nitrate) and a fuel (e.g. glycine, hydrazine). First, reactants are dissolved in water and the obtained solution thoroughly mixed, to reach essentially molecular level homogenization of the reaction medium. After preheating to boiling point of water and its evaporation, the solution can be ignited or self-ignites and temperature rises rapidly (up to 10⁴ °C s⁻¹) to values as high as 1500 °C. This high temperature for short period of time converts the initial mixture typically to fine well-crystalline powder of desired composition. As a result, calcination step, which adversely affects the powder surface area and related properties, can be eliminated.

The families of nano-oxides synthesized using aqueous combustion approach include binary oxides (e.g. Fe₂O₃,

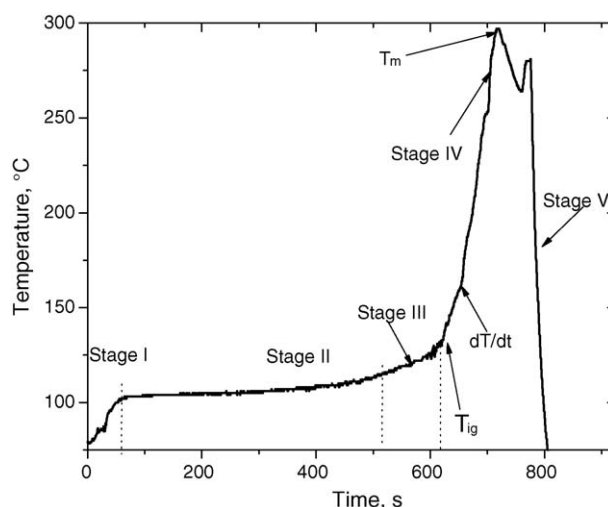
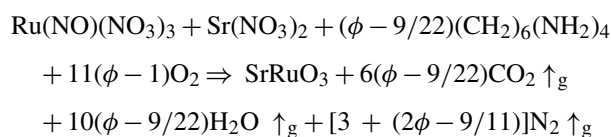


Fig. 1. Typical temperature–time profile during aqueous CS [20].

Fe₃O₄, RuO₂), perovskites (e.g. LaFeO₃, SmCoO₃, SrRuO₃, La_{0.8}Sr_{0.2}Fe_{1-x}Ni_xO₃, La_{0.8}Sr_{0.2}CrO₃) and cuprates (e.g. La₂CuO₄). These catalysts were synthesized in a chemical reactor made of quartz, which allows one to conduct experiments in different ambient atmospheres (i.e. air, oxygen, argon), measurements of temperature–time history of the reaction, and process monitoring by digital camera (Panasonic Digital Camcorder, Model PV-DV103). The temperature was measured using type K thermocouples (Omega Engineering Inc.), attached to a multi-channel acquisition system (INET-200 controller card, Omega Engineering Inc.) with rates from 5 to 60 samplings s⁻¹.

For example, under equilibrium conditions, the reaction for strontium–ruthenium-based system using hexamethylene tetra amine as fuel can be represented as follows:



Note that ϕ represents the fuel: oxidizer ratio. It equals 1 when the oxygen released by the nitrates is sufficient for complete oxidation of the fuel, with none required from the atmosphere.

After reactants dissolution in sufficient amount of water and thorough mixing, the solution was preheated uniformly at rate $\sim 5 \text{ K min}^{-1}$ up to the water boiling point (stage I, Fig. 1). This was followed by a relatively long ($\sim 5 \text{ min}$) constant temperature region during which all free and partially bound water evaporated (stage II, Fig. 1). The next stage was characterized by higher heating rates ($\sim 12 \text{ K min}^{-1}$, stage III, Fig. 1) and ended (at some ignition temperature, T_{ig}) with either sudden (at some ignition temperature, T_{ig}) uniform temperature rise to a maximum value, T_{m} , or reaction initiated in a specific hot spot followed by steady wave propagation along the mixture (stage IV, Fig. 1). The rate of temperature change in this so-called combustion zone for different reactant systems was in the range $10\text{--}10^4 \text{ K s}^{-1}$, with the process duration varying from 10 to 10^2 s . After cooling (stage V), the synthesized products were fine and typically crystalline solid powders.

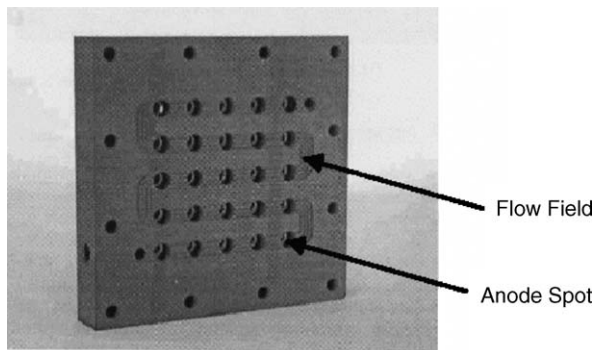


Fig. 2. Anode flow field for NuVant system.

The obtained products were analyzed for phase composition and crystallinity using X₁ Advanced diffraction system (Scintag Inc.). The powder microstructure was studied by field emission scanning electron microscopy (Hitachi, Model S-4500) and the specific surface area was measured using BET analysis (Autosorb 1C, Quantachrome Instruments). Quantitative elemental analysis was carried out using Optima 3300 XL inductively coupled plasma atomic emission spectrometer (ICP-AES Perkin-Elmer).

2.2. Catalyst screening

The electrochemical screening system, NuVant 100P developed by Liu and Smotkin [15], consists of an array of 25 individually controlled electrodes (Fig. 2). Fuel such as methanol is introduced through serpentine flow field channels and the membrane electrode assembly (MEA) represents a miniaturized fuel cell for power generation. Thus, by using the above system, one can obtain the anode polarization curves simultaneously for 25 different cells. Note that hydrogen is delivered to a common platinum cathode, which has a large surface area ($\sim 100 \text{ cm}^2$) and thus acts as a nonpolarizable reference electrode. More details of the system can be found elsewhere [15].

The MEA fabrication involved several steps. First, the well-dispersed anode, cathode and special carbon inks were prepared. For anode inks, synthesized oxide powders (pure or with desired amount of Pt-black) as well as standard catalysts, i.e. Pt–Ru (stock # 41171, Alfa Aesar) were thoroughly stirred in a suitable solvent (e.g. methanol and *iso*-propanol) for several hours. Similar procedure was used to prepare the cathode, i.e. Pt-black (stock # 12755, Alfa Aesar) and carbon (stock # 39723, Alfa Aesar) inks.

In the next stage, carbon paper (TGPH060 DeNora North America Inc.) was used as gas diffusion layer. However, since the initial paper porosity was too large ($\sim 80\%$) for optimum catalyst deposition, to increase its anode electronic conductivity, carbon ink was coated on its surface with 1 mg cm^{-2} loading. The different inks were then painted on such supports to desired loadings to produce a variety of anode electrodes and a cathode. The catalyst loadings were optimized based on the surface coverage of the prepared inks. A typical example is shown in Fig. 3. For the same loading of 4 mg cm^{-2} , Pt–Ru anode showed uniform coverage (Fig. 3a), while for SmCoO_3 it did not yield similar results

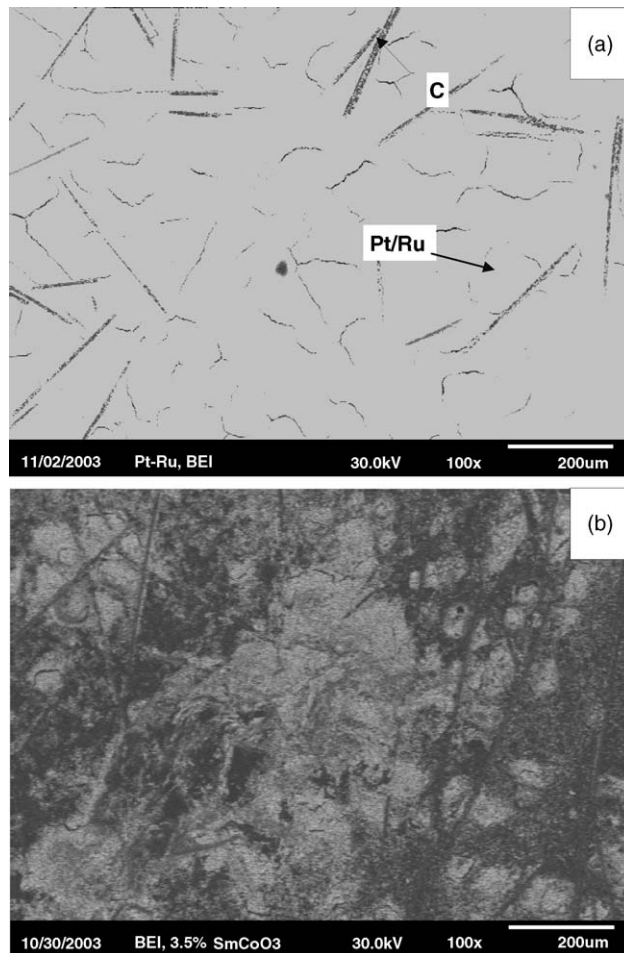


Fig. 3. Catalysts deposited on carbon supported toray paper: (a) Pt–Ru BEI 130 \times and (b) SmCoO_3 BEI 130 \times .

(Fig. 3b). Using these results, loading optimization for different compositions, to obtain uniform catalyst distribution on the gas diffusion layer, was carried out.

Finally, the anodes, electrolyte (Nafion 117) and cathode were hot pressed at 160°C under a load $\sim 10^3 \text{ lb}$ to fabricate the MEA which, as mentioned above, consisted of 25 different individually controlled anodes and a reference cathode. Maintaining the cathode at a fixed potential, the anode polarization (I – V) curves were obtained by varying the anode potentials and measuring the generated currents. Note that the data was obtained at 90°C , 14 ml min^{-1} methanol flow rate and 2 mV s^{-1} scan rate, unless specified otherwise.

3. Results and discussion

3.1. Catalyst synthesis

The surface areas and phase compositions of the investigated compositions are presented in Table 1. During the preparation, the effects of different reaction parameters including fuel type, ambient atmosphere and precursors on the product composition and properties, as elaborated recently for the iron oxide system [21], were also studied to understand the reaction mechanism.

Table 1
Properties of compositions synthesized for catalyst screening

Sample	BET surface area ($\text{m}^2 \text{g}^{-1}$)	Phase composition	
1	RuO ₂	17	RuO ₂
2	Pt–Ru standard	68	Pt–Ru
3	SrRuO ₃	~2	SrRuO ₃
4	γ -Fe ₂ O ₃	28	γ -Fe ₂ O ₃
5	SmCoO ₃	2	SmCoO ₃
6	Fe ₃ O ₄	45	Fe ₃ O ₄
7	LaFeO ₃	4	LaFeO ₃
8	La _{0.8} Sr _{0.2} CrO ₃	35	La _{0.8} Sr _{0.2} CrO ₃
9	1% Pt inclusion in SrRuO ₃ during synthesis	10	SrRuO ₃ , Pt and some unreacted Sr(NO ₃) ₂
10	5% Pt inclusion in SrRuO ₃ during synthesis	15	SrRuO ₃ , Pt and some unreacted Sr(NO ₃) ₂
11	La ₂ CuO ₄	4	La ₂ CuO ₄

Among all the samples studied, SrRuO₃-based compositions showed the most promising catalytic performance under DMFC conditions. For this reason, this system was investigated in detail. In addition, the effect of Pt incorporation into perovskite-based catalyst, either during synthesis or externally during ink preparation, was also studied. In the sequel, samples prepared by addition of Pt during aqueous combustion synthesis will be referred to as *internal*, while those using Pt at ink preparation stage as *external*. Table 2 gives a comparison of the Pt–Ru standard with different combinations for the basic SrRuO₃ catalyst, along with the respective Pt and Ru contents. The last column reflects the cost of the noble metals (i.e. Pt and Ru), present either within the perovskite structure or as external additive per unit anode area. It appears that for equivalent catalytic performance, as compared with Pt–Ru standard, some cost savings may be achieved by use of SrRuO₃ in all investigated cases.

3.2. Measurement of catalyst performance

The catalytic properties of synthesized compositions, obtained by the rapid screening approach (NuVant system), for methanol electro-oxidation are presented and discussed next. To compare the obtained data with previously reported values and thus confirm the accuracy of the applied technique, the results for standard Pt–Ru and Pt–black are also considered.

Table 2
Pt content for SrRuO₃-based system

Composition	Loading (mg cm^{-2})	Pt (mg cm^{-2})	Ru (mg cm^{-2})	Cost ($\text{\$ cm}^{-2}$)
Pt–Ru	4	2	2	0.32
SrRuO ₃	15	0	6.3	0.25
SrRuO ₃ + 1% internal Pt	15	0.15	6.3	0.26
SrRuO ₃ + 5% internal Pt	15	0.6	6.3	0.30
SrRuO ₃ + 1% external Pt	15	0.15	6.3	0.26
SrRuO ₃ + 5% external Pt	15	0.75	6.3	0.318

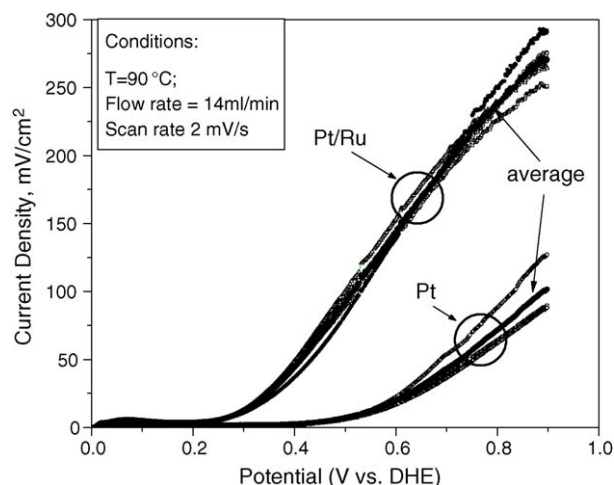


Fig. 4. Typical I - V response for standard Pt–Ru and Pt samples using NuVant system.

3.2.1. Pt-based catalysts

Fig. 4 shows typical current–potential curves obtained with Pt–Ru and Pt–black during an experimental run, where each curve corresponds to a specific anode spot in the MEA. The curves in each group show similar behavior, indicating the reproducibility of the results with a variation of $\sim 10\%$ in the voltage range 0–0.6 V. The average I - V curves, based on the statistical analysis of multiple individual sample spots, are also presented.

It can be seen that the oxidation reactions for Pt–Ru start at ~ 0.22 V, while significantly larger over-potential is observed for Pt–black. Further, the current densities are in good agreement with literature data for these catalysts (cf. [6,15,22]). The above results support the conclusion [15] that the experimental system adequately characterized the catalytic activities of tested samples and could be a powerful tool in rapid search for the best composition.

3.2.2. Perovskite catalyst

As noted in Section 3.1, among the various families of investigated compounds, it was found that SrRuO₃-based perovskites possess the most promising catalytic performance. A comparison of average I - V curves for Pt–Ru, SrRuO₃ and a blank run with deionized water under same experimental conditions is shown in Fig. 5. It can be seen that while for Pt–Ru, current increases monotonically in the potential range 0.2–0.6 V, for perovskite catalyst a maximum is observed at ~ 0.35 V. Although no direct data is available on oxidation potential of SrRuO₃, the values for RuO₂ and Sr provide some insight into the stability of the sample. The standard electrode potential of RuO₂ (Ru in the same oxidation state as in SrRuO₃) is ~ 1.15 V, while that of Sr is -2.88 V [23]. Since all trials were conducted in the voltage range 0–0.8 V, one may conclude that the observed current densities are due to the catalytic decomposition of fuel on this electrochemically stable composition. Further, a comparison of blank run data (curve 3), with typical methanol involved I - V curves (curve 2) support the above conclusion that the second peak for perovskite catalyst is a result of methanol electro-oxidation reaction.

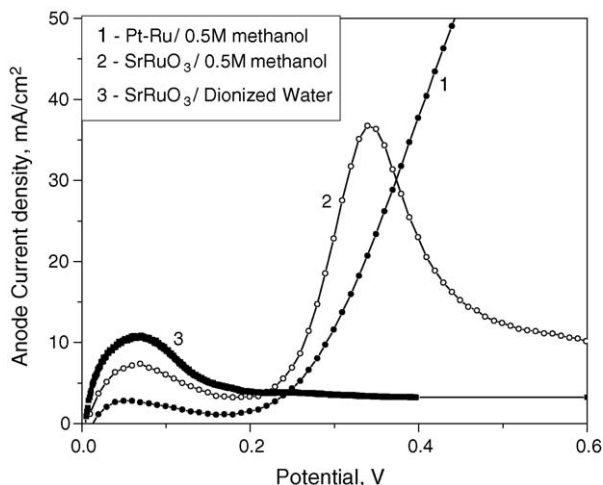


Fig. 5. Typical I - V response for SrRuO_3 sample and DI water at 90°C and 14 ml min^{-1} flow rate.

3.2.3. Electro-oxidation mechanism

To understand the non-monotonic I - V behavior of perovskite compositions, additional experiments were conducted with different fuels such as CO and H_2 . The typical I - V curve for CO electro-oxidation on SrRuO_3 is shown in Fig. 6a (curve 2).

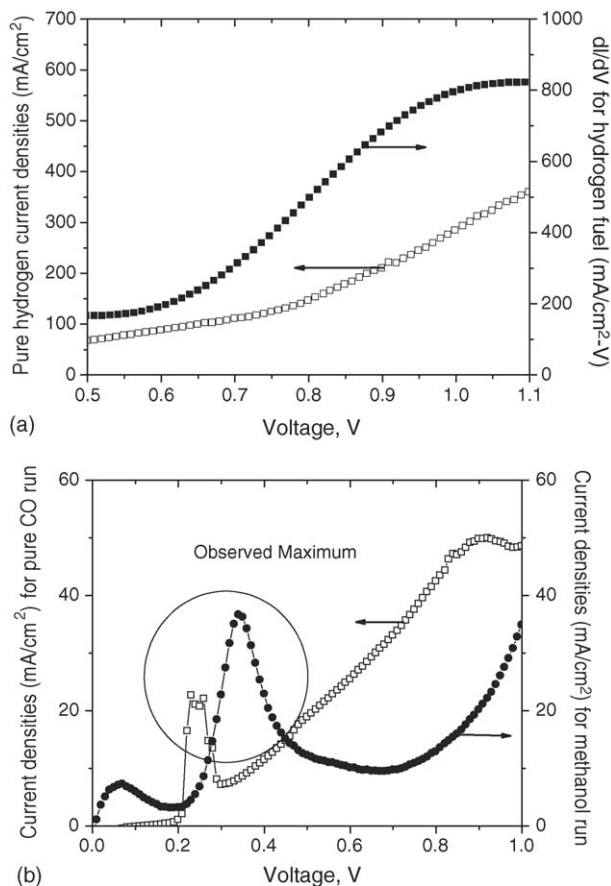


Fig. 6. SrRuO_3 performance in different atmospheres at 90°C and 14 ml min^{-1} flow rate: (a) carbon monoxide and methanol and (b) hydrogen and its corresponding dI/dV .

It is interesting that this dependence also has a current maximum in the potential range 0.2–0.4 V. For hydrogen oxidation (Fig. 6b) on the same perovskite catalyst, the current density rises along the entire investigated potential range, however the rate of current change increases significantly at potentials beyond 0.7 V.

Since the characteristic maximum is observed in the same voltage range for both methanol and CO fuels, one may conclude that this behavior of the I - V curve for DMFC is likely related to CO generated during last step of well-known methanol oxidation mechanism [24]. Further, the increased current densities beyond 0.8 V for this perovskite may be explained by the observed increase in current values for the hydrogen run (Fig. 6b). Specifically, methanol oxidation rate and hence intermediate hydrogen generation may increase at higher potential because of higher driving force. However, detailed studies are required to substantiate this claim and experiments are under progress to understand the mechanism.

Based on the above results, the nature of SrRuO_3 curve in DMFC is explained next. Curve 3 of Fig. 5 indicates that the first peak may be due to water oxidation. The existence of second peak can be reasoned as follows. Initially the catalyst shows good oxidation of the fuel resulting in increased current densities. However, as the reaction progresses, intermediate CO may get strongly adsorbed on the surface resulting in lower reaction rates and hence a decrease in the current density leading to the second peak. For higher V , current density may increase due to enhanced methanol oxidation and subsequent intermediate hydrogen generation as proposed in the preceding paragraph.

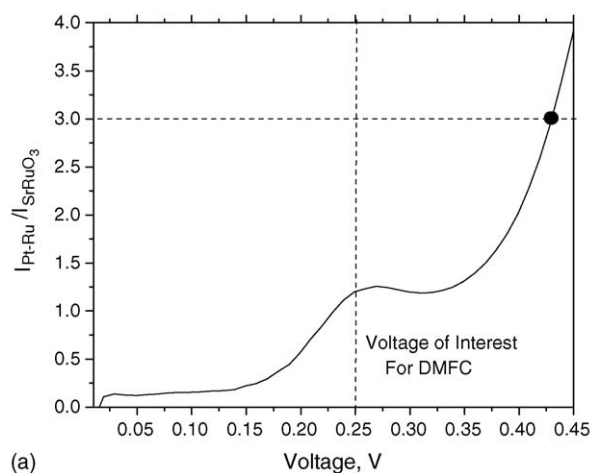
3.2.4. Comparison of pure SrRuO_3 and Pt-Ru catalysts

It is interesting to compare the behaviors of Pt-Ru and SrRuO_3 catalysts, in the potential range 0.2–0.4 V, which is of interest for DMFC applications. First, note that the reaction overpotentials for both are similar ($\sim 0.2\text{ V}$) (Fig. 5). Also, it can be seen that these catalysts show comparable activities in the potential range 0.25–0.35 V (see Fig. 7a). In addition, it was observed (see Fig. 7b) that the current for SrRuO_3 is more stable (8% drop) than for Pt-Ru (16% drop) at 0.4 V.

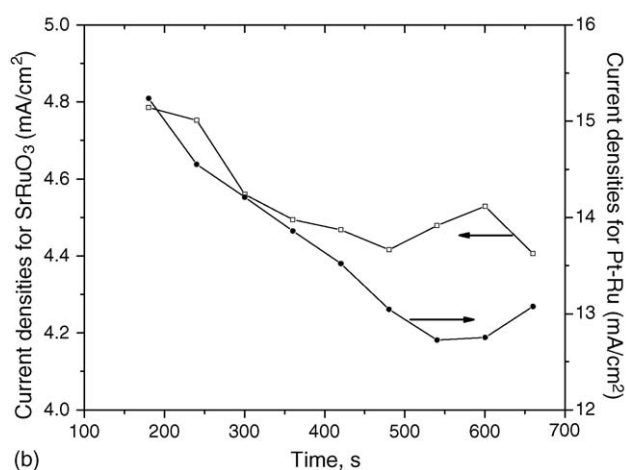
While comparably active at low anode potential and exhibiting good performance stability, the absolute values of current densities for pure SrRuO_3 catalysts are relatively low (up to 4 mA cm^{-2}). This, coupled with a drop in activity at higher potentials ($>0.35\text{ V}$) makes the material less attractive than Pt-Ru.

3.2.5. Partially substituted perovskite catalysts

3.2.5.1. Performance comparison. To combine the advantages of good catalytic activity of SrRuO_3 at lower potential and of Pt-Ru at higher voltage, Pt was added to SrRuO_3 during synthesis (internal Pt) and also externally during ink preparation. As explained below, various Pt loadings added to SrRuO_3 were investigated and the results are shown in Fig. 8, which led to some important conclusions. First, a significant increase in activity is observed with addition of 1 and 5 wt.% Pt. This effect



(a)

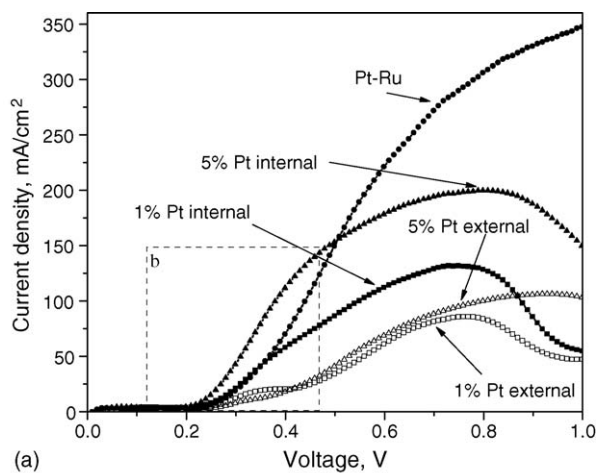


(b)

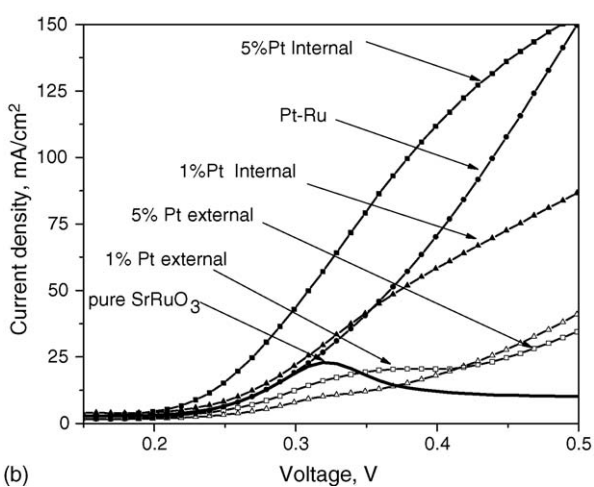
Fig. 7. Performance comparison for SrRuO_3 and Pt–Ru at 90°C and 14 ml min^{-1} flow rate: (a) $I_{\text{Pt-Ru}}/I_{\text{SrRuO}_3}$ as a function of applied voltage and (b) chronoamperometric data at 0.42 V .

was also observed by Yue et al. [4] for Pt added externally to SrRuO_3 . These authors measured the properties only for Pt added externally to SrRuO_3 samples, while in the present study the catalytic performance of samples was measured as a function of preparation technique (i.e. internal and external Pt) and loading. Second, partially substituted perovskite catalyst with 5% internal Pt loading exhibits lower over potential than the Pt–Ru standard. Finally, note that Pt added during synthesis (internal) is more effective than when incorporated externally during ink preparation stage, leading to better performance even at lower Pt loading and resulting in significant cost savings as shown in Table 2. This is most likely due to the more uniform distribution of Pt within the structure during the aqueous combustion synthesis.

To verify that the enhanced activity of substituted perovskite is related to its specific structure and not Pt alone, additional experiments were conducted with different platinum loadings. It was observed (see Fig. 9) that the SrRuO_3 perovskite with Pt loading 0.15 mg cm^{-2} is superior to catalyst containing 1 mg cm^{-2} Pt alone. Further, reaction over-potential is lower for all SrRuO_3 -based catalysts than for platinum. For example at Pt loading of 0.25 mg cm^{-2} , the reaction initiates at



(a)



(b)

Fig. 8. Performance comparison for different SrRuO_3 -based and standard Pt–Ru catalysts: (a) $0\text{--}1.2\text{ V}$ and (b) $0\text{--}0.5\text{ V}$.

$\sim 0.34\text{ V}$, while for 0.15 mg cm^{-2} Pt loading in SrRuO_3 , it starts at $\sim 0.25\text{ V}$. The above two effects unequivocally confirm that the performance enhancement owes to the combination of SrRuO_3 and Pt.

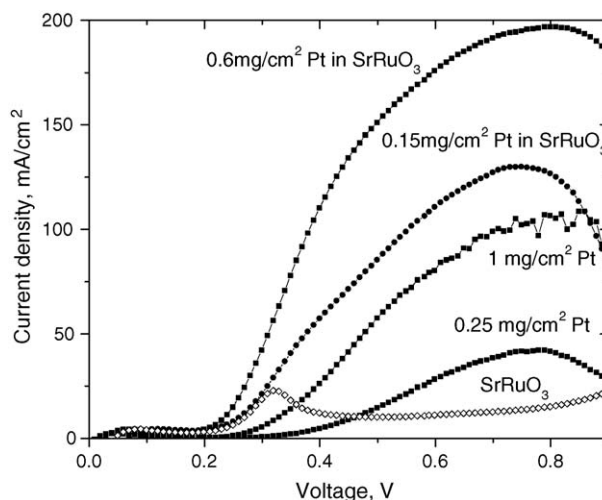
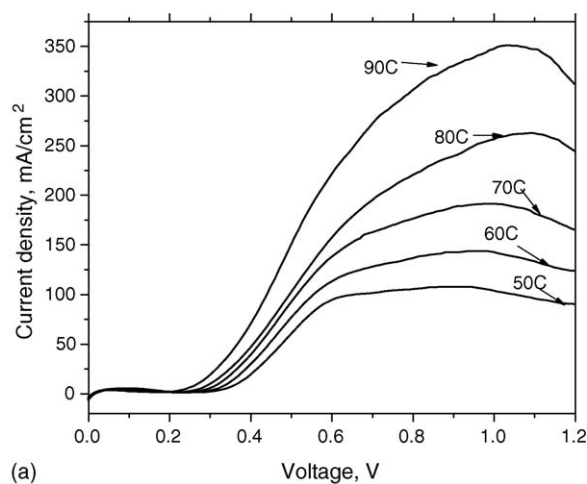
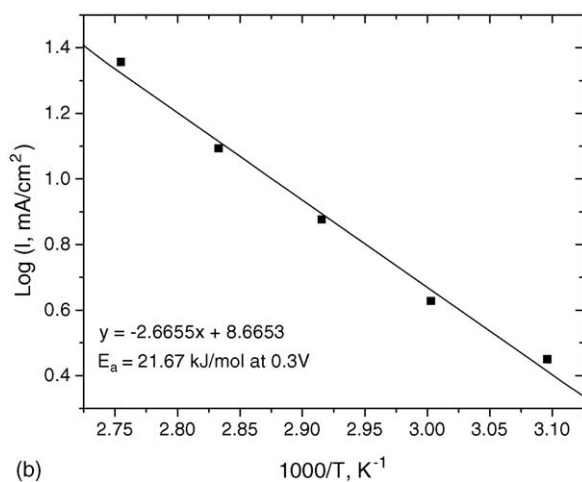


Fig. 9. Performance comparison for Pt catalyst with and without SrRuO_3 at 90°C and 14 ml min^{-1} flow rate.



(a)

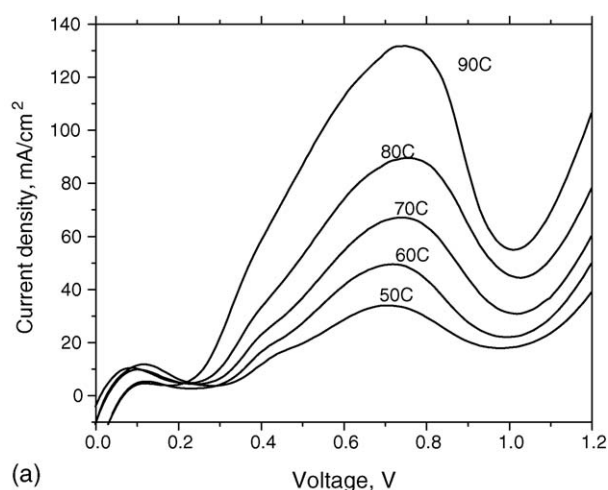


(b)

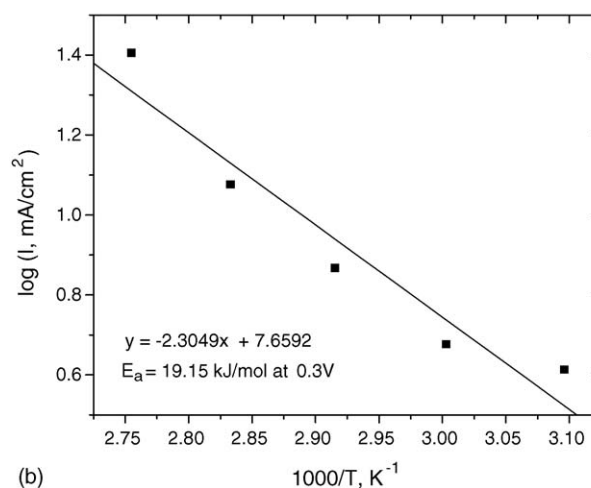
Fig. 10. Temperature dependence for Pt–Ru catalyst: (a) 0–1.2 V and (b) activation energy computation at 0.3 V.

As noted earlier, the effects of different operational conditions, including temperature and methanol flow rate, were also studied and are described next.

3.2.5.2. Effect of temperature and estimation of activation energy. The anode polarization curves for Pt–Ru and Sr-based perovskite catalysts with 1 wt.% internal Pt were obtained as a function of temperature and results are shown in Figs. 10a and 11a, respectively. It can be seen that in both cases, methanol oxidation rates increase with increasing temperature. Using such dependence at a constant anode potential (e.g. 0.3 V), one can develop Arrhenius plots and compute the activation energy (see Figs. 10b and 11b). The activation energy for Pt–Ru (~ 22 kJ mol⁻¹) obtained by this approach is lower than previously reported data (~ 60 kJ mol⁻¹) [25]. This may be attributed to the presence of Nafion coated electrodes in the current studies, which enhance the methanol oxidation kinetics [26]. It is interesting that the E_a values obtained for SrRuO₃-based compositions are also of similar order (see Table 3). Thus, the difference in current densities (Fig. 8) suggests that the nature of the catalyst influenced either the Arrhenius preexpo-



(a)



(b)

Fig. 11. Temperature dependence for SrRuO₃ catalyst with 1 wt.% Pt internal SrRuO₃: (a) 0–1.2 V and (b) activation energy computation at 0.3 V.

ponential factor or the concentration dependence of the reaction rate.

3.2.5.3. Effect of methanol flow rate. While the effects of temperature were similar for all samples, they behaved differently with varying methanol flow rate. For Pt–Ru, as well as for 1 and 5 wt.% internal Pt in SrRuO₃, increasing flow rate increased the saturation current densities (see Fig. 12a, c and d). The results indicate that for these catalysts, at higher voltage, the reaction is mass transport limited. For SrRuO₃, however (Fig. 12b) the saturation current densities remained essentially unchanged, suggesting that its performance is likely to be kinetically controlled.

Table 3
Activation energies for different samples at 0.3 V

Sample	Activation energy (kJ mol ⁻¹)
Pt–Ru	22
SrRuO ₃ + 1% internal Pt	19
SrRuO ₃ + 5% internal Pt	24
SrRuO ₃	20

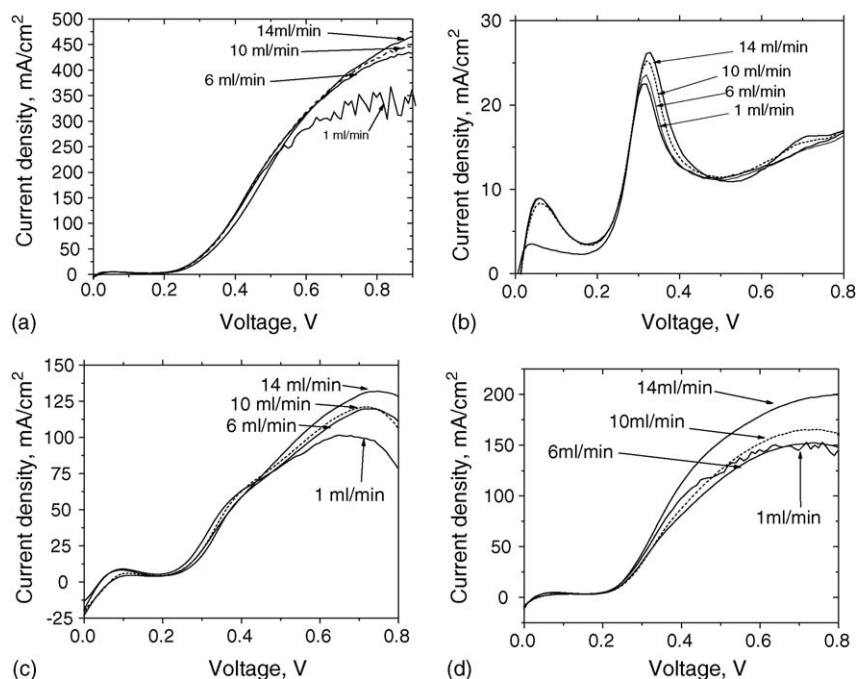


Fig. 12. Effect of methanol flow rate on catalyst performance at 90 °C: (a) Pt–Ru, (b) SrRuO₃, (c) 1 wt.% internal Pt SrRuO₃ and (d) 5 wt.% internal Pt SrRuO₃.

4. Concluding remarks

In the current work, a high throughput approach for synthesis and screening of catalysts for direct methanol fuel cell application was utilized. This method involved (a) energy efficient and fast synthesis of a library of compounds using the aqueous combustion synthesis (CS) technique, and (b) rapid catalyst screening using the high throughput NuVant system.

A variety of high surface area catalysts were synthesized and tested. It was found that the Sr-based perovskites showed performance comparable with standard Pt–Ru. Further, it was observed that the method of doping SrRuO₃ with Pt influenced the activity. Specifically, platinum added *during* aqueous CS yielded better catalyst than when added externally at the ink preparation stage. Finally, it was also demonstrated that the presence of SrRuO₃ significantly enhanced the catalytic activity of Pt, leading to superior performance even at lower noble metal loadings.

The better activity of SrRuO₃ containing Pt can be attributed to the high surface area and uniform phase composition obtained owing to the advantages of aqueous CS, viz., mixing on the molecular level and under the unique conditions of rapid high-temperature reactions. Thus, the method described here is a promising approach for catalyst synthesis and screening for fuel cell applications.

Acknowledgements

This work was supported by the U.S. Army CECOM RDEC through Agreement DAAB07-03-3-K414. Such support does not constitute endorsement by the U.S. Army of the views expressed in this publication. We are also grateful to NSF (grant CTS-0446529) for support of this research. Finally, we thank

Prof. Elizabeth Podlaha-Murphy for useful technical discussions in interpreting the results.

References

- [1] L. Carrette, K.A. Friedrich, U. Stimming, *Chem. Phys. Chem.* 1 (2000) 162–193.
- [2] B.D. McNicol, D.A.J. Rand, K.R. Williams, *J. Power Sources* 83 (1999) 15–31.
- [3] J. White, F. Sammels, *J. Electrochem. Soc.* 140 (1993) 2167–2177.
- [4] Z. Yue, Y. Zhanhui, Z. Hengbin, C. Xuejing, L. Shujia, S. Chiachung, *Mater. Chem. Phys.* 57 (1999) 285–288.
- [5] V. Raghuvver, B. Viswanathan, *Fuel* 81 (2002) 2191–2197.
- [6] H.-C. Yu, K.-Z. Fung, T.-C. Guo, W.-L. Chang, *Electrochim. Acta* 50 (2004) 811–816.
- [7] J. Larminie, A. Dicks, *Fuel Cell Systems Explained*, John Wiley, Chichester, 2000, pp. 66–67.
- [8] S. Surampudi, S.R. Narayanan, E. Vamos, H. Frank, G. Halpert, A. LaConti, J. Kosek, G.K. Surya Prakash, G.A. Olah, *J. Power Sources* 47 (1994) 377–385.
- [9] G. Tremiliosi-Filho, H. Kim, W. Chrzanowski, A. Wieckowski, B. Grzybowska, P. Kulesza, *J. Electroanal. Chem.* 467 (1999) 143–156.
- [10] Y.C. Liu, X.P. Qui, Y.Q. Huang, W.T. Zhu, *Carbon* 40 (2002) 2375–2380.
- [11] Z. He, J. Chen, D. Liu, H. Tang, W. Deng, Y. Kuang, *Mater. Chem. Phys.* 85 (2004) 396–401.
- [12] A.S. Arico, A.K. Shukla, K.M. El-Khatib, P. Creti, V. Antonucci, *J. Appl. Electrochem.* 29 (1999) 671–676.
- [13] C.K. Witham, W. Chun, T.I. Valdez, S.R. Narayanan, *Electrochim. Solid State Lett.* 3 (2000) 497–500.
- [14] D.L. Boxall, G.A. Deluga, E.A. Kenik, W.D. King, C.M. Lukehart, *Chem. Mater.* 13 (2001) 891–900.
- [15] R. Liu, E.S. Smotkin, *J. Electroanal. Chem.* 535 (2002) 49–55.
- [16] K.C. Patil, S.T. Aruna, T. Mimami, *Curr. Opin. Solid State Mater. Sci.* 6 (2002) 507–512.
- [17] Varma, A.S. Mukasyan, K.T. Deshpande, P. Pranda, P.R. Erri, *MRS Fall meeting Symposium Proceedings on Synthesis, Characterization*

- and Properties of Energetic/Reactive Nanomaterials, vol. 800, 2003, pp. 113–124.
- [18] K. Deshpande, A. Mukasyan, A. Varma, *J. Am. Ceram. Soc.* 86 (2003) 1149–1154.
- [19] G.R. Rao, H.R. Sahu, B.G. Mishra, *Colloids Surf. A* 220 (2003) 261–269.
- [20] C. Hwang, T. Wu, *J. Mater. Sci.* 39 (2004) 6111–6115.
- [21] K. Deshpande, A. Mukasyan, A. Varma, *Chem. Mater.* 16 (2004) 4896–4904.
- [22] H. Dohle, K. Wippermann, *J. Power Sources* 135 (2004) 152–164.
- [23] D.R. Lide (Ed.), *CRC Handbook of Chemistry and Physics*, 85th ed., CRC Press LLC, New York, 2004–2005, pp. 8–27.
- [24] E.S. Smotkin, R.R. Diaz-Morales, *Annu. Rev. Mater. Res.* 33 (2003) 557–579.
- [25] E.A. Batista, H. Hoster, T. Iwasita, *J. Electroanal. Chem.* 554–555 (2003) 265–271.
- [26] B. Gurau, E.S. Smotkin, *J Power Sources* 112 (2002) 339–352.